Predicting evapotranspiration from drone-based thermography – a method comparison in a tropical oil palm plantation

Florian Ellsäßer[1], Christian Stiegler[2], Alexander Röll[1], Tania June[3], Hendrayanto[4], Alexander Knohl[2,5], Dirk Hölscher[1,5]

[1] University of Goettingen, Tropical Silviculture and Forest Ecology, Büsgenweg 1, 37077 Göttingen, Germany

[2] University of Goettingen, Bioclimatology, Büsgenweg 2, 37077 Göttingen Germany

[3] Bogor Agricultural University, Geophysics and Meteorology, Jln. Meranti, 16680 Bogor, Indonesia

[4] Bogor Agricultural University, Forest Management, Kampus IPB Darmaga, 16680 Bogor, Indonesia

[5] University of Goettingen, Centre of Biodiversity and Sustainable Land Use, Platz der Göttinger Sieben 5, 37073 Göttingen, Germany

Correspondence to: Florian Ellsäßer (fellsae@gwdg.de)

Abstract

For the assessment of evapotranspiration, near-surface airborne thermography offers new opportunities for studies with high numbers of spatial replicates and in a fine spatial resolution. We tested drone-based thermography and the subsequent application of three energy balance models (DATTUTDUT, TSEB-PT, DTD) using the widely accepted eddy covariance technique as a reference method. The study site was a mature oil palm plantation in lowland Sumatra, Indonesia. For the 61 flight missions, latent heat flux estimates of the DATTUTDUT model with measured net radiation agreed well with eddy covariance measurements (r^2=0.85; MAE=47; RMSE=60) across variable weather conditions and daytimes. Confidence intervals for slope and intercept of a model II Deming regression suggest no difference between drone-based and eddy covariance method, thus indicating interchangeability. TSEB-PT and DTD yielded agreeable results, but all three models are sensitive to the configuration of the net radiation assessment. Overall, we conclude that drone-based thermography with energy-balance modeling is a reliable method complementing available methods for evapotranspiration studies. It offers promising, additional opportunities for fine grain and spatially explicit studies.

1 Introduction

Evapotranspiration (ET) is a central flux in the hydrological cycle on a regional and on a global scale. Terrestrial ET consumes almost two-thirds of terrestrial precipitation (Oki and Kanae, 2006). There is an interest in better understanding ET and its drivers as climate change is expected to increase atmospheric evaporative demand and droughts are predicted to become more severe and frequent in the future (Prudhomme et al., 2014). ET is also strongly affected by land-cover and land-use changes, which are currently very pronounced in tropical regions (Hansen et al., 2013).

The eddy covariance technique (EC) is a widely accepted and well-established method to quantify ET at the stand scale (Baldocchi et al., 2001; Fisher et al., 2017). It results in a single latent heat flux (LE) value integrated over the footprint of the EC tower at a given time that can be converted to an ET estimate. A spatial fine grain attribution of different surface patches to this overall ET value is generally not possible. The EC method is costly and labor intensive, and therefore, a relatively low number of spatial replicates within a given region and among its different ecosystems are typically available. The EC method also has certain constrains regarding topography, atmospheric turbulence and landscape heterogeneity (Göckede et al., 2008).

A complementary approach for assessing LE at larger spatial scales is the use of remotely sensed land surface temperatures (LST) as boundary conditions for energy balance modeling and subsequent conversion to ET (Brenner et al., 2017; Guzinski et al., 2014; Hoffmann et al., 2016; Ortega-Farías et al., 2016; Xia et al., 2016). Transpiration from leaf surfaces leads to evaporative cooling of the canopy; LSTs, along with air temperature, can thus be used as a reliable indicator of plant water use, both in monocultures and in spatially highly heterogeneous systems such as natural forests (Lapidot et al., 2019). Compared to the EC method, this approach can potentially increase the number of spatial replicates within and among ecosystems and is also applicable in challenging terrain. Remotely sensed LSTs are regarded as good indicators for plant water use, stress and transpiration (Jones and Vaughan, 2010). One approach to obtain LST data is the use of satellite-based observations (Allen et al., 2007; Bastiaanssen et al., 1998; Ershadi et al., 2013). However, the spatial resolution of satellite data such as Landsat TM, ASTER, MODIS or AVHRR ranges from 90 m to 1 km, limiting the distinction of plant canopies and soil (Berni et al., 2009). A higher temporal resolution of satellite-based thermal infrared (TIR) observations is usually associated with a lower spatial resolution, and TIR data from satellites in both high spatial and high temporal resolution are not yet available (Brenner et al., 2017). Additionally, clouds are barriers for thermal radiation and therefore have a strong effect on the quality and availability of satellite-based TIR observations (Guzinski et al., 2013). This is of particular importance in regions with frequent cloud cover such as in tropical environments.

An alternative, recently emerging approach to measure LSTs is the use of drones. Radiometric TIR sensors for LST recording have become light-weight and affordable, and drones are now capable of carrying adequate payloads for reasonable timespans. Near-surface thermography-based studies allow temporal resolutions in flexible, e.g. hourly time steps and a spatial resolution in the decimeter scale or finer. Drone-based TIR recording and subsequent modeling of LE with energy balance models has previously shown promising results for short grass and crop vegetation in Central Europe (Brenner et al., 2018; Hoffmann et al., 2016). However, remote sensing of LST from drones is challenging and involves careful planning. Recording LST close to the surface results in a high resolution but reduces the area covered in a certain time span compared to surveying from a higher altitude. Increasing flight altitude reduces spatial resolution of LST images and thus increases the averaging of surface temperatures from individual canopies, soil patches and branches from neighboring canopies into a single pixel (Still et al., 2019). Further, air humidity can have a major effect on measurement accuracy as water vapor does not only attenuate the signals from the surface of interest to the sensor, but also emits its own thermal radiation (Still et al., 2019).

Different energy balance models are available to compute LE from LST and subsequently calculate ET. In the one-source energy balance model DATTUTDUT (Deriving Atmosphere Turbulent Transport Useful To Dummies Using Temperature) (Timmermans et al., 2015) fluxes are estimated by relating single pixel temperatures to local temperature extremes. Two-source energy balance models such as TSEB (Two-Source Energy Balance) (Norman et al., 1995) and DTD (Dual Temperature Difference) (Norman et al., 2000) divide measured LSTs into a vegetation and a soil fraction. Several adaptions of these models were developed; the TSEB-PT model as described in Hoffmann et al. (2016), uses the Priestley-Taylor coefficient (PT) to determine canopy H flux and subsequently calculate the other fractions from the surface energy balance. TSEB-PT is based on the temperature difference between LST and air temperature (Norman et al., 1995). Expanding this concept, DTD uses a dual-temperature difference from an additional early morning set of measurements to account for biases in remotely sensed LSTs (Hoffmann et al., 2016; Norman et al., 2000). Crucial in applying such energy balance models is how the net radiation (Rn) is implemented. In the original formulation of the DATTUTDUT model Rn is fully modeled, assuming a range of prerequisites and environmental conditions (Timmermans et al., 2015). TSEB-PT and DTD models use measured short and long-wave radiation to estimate Rn as a sum of in- and outgoing long- and short-wave radiation (Norman et al., 1995, 2000). Using airplanes or drones to record LSTs, the three models previously showed promising results for grass and crop surfaces in temperate and subtropical regions (Brenner et al., 2017, 2018; Hoffmann et al., 2016; Xia et al., 2016). However, to our knowledge, a comprehensive method comparison considering potential errors in both a reference method (e.g. the EC technique) and novel drone-based approaches is not yet available. Since full method comparisons based on model II regression require a sample size of at least n=60 data pairs (Legendre and Legendre, 2003), many previous studies with smaller sample sizes were constrained to

112 using error terms and correlation coefficients.

113

114 The current study was conducted in the lowlands of Jambi province (Sumatra, Indonesia) where over the
115 last decades, large areas of rainforest have been converted to rubber and oil palm plantations (Clough et
116 al., 2016; Margono et al., 2012). This resulted in regional-scale changes in transpiration (Röll et al., 2019)
117 and land surface warming (Sabajo et al., 2017). We assessed energy fluxes in a mature monoculture oil
118 palm plantation and compared the LE estimates of drone-based methods with the established EC method
119 as measured ground-based reference. Three energy-balance models (DATTUTDUT, TSEB-PT, DTD)
120 were tested, each with three different configurations for the determination of Rn (fully modeling Rn, Rn
121 estimates based on short-wave irradiance and measuring Rn). The objectives of our study were to compare
122 LE estimates from the drone-based methods to the EC technique, with a special focus on the detection of
123 proportional and continuous errors among the methods and an evaluation of the model's prediction
124 performance. The present study focuses on the comparison of different drone-based methods as a baseline
125 for future ecological studies, rather than applying the methods to different land-use types.

126

127 **2 Methods**

128

129 **2.1 Study site**

130

131 The study site is located in the lowlands of Jambi province (Sumatra, Indonesia) near the equator (E
132 103.3914411, N -1.6929879, 76 m a.s.l.). Average annual air temperature in the region is 26.5°C and
133 average annual precipitation is 2235 mm yr^{-1} (Drescher et al., 2016). At the time of our measurement
134 campaign in August 2017, the studied monoculture oil palm (*Elaeis guineensis*) plantation was 15 years
135 old. Palm stem density was 140 palms ha^{-1}, with an average palm height of 14.3 m and an average canopy
136 radius of 4.5 m. Leaf area index (LAI) was estimated at 3.64 $m^2\,m^{-2}$ (Fan et al., 2015) and canopy cover
137 was estimated to be 90%. Plantation management included the removal of older and non-vital leaves from
138 the oil palms, herbicide application to remove most understory plants and fertilization (196 kg N ha^{-1} yr^{-1}
139 ^{1}) (Meijide et al., 2017). The average annual oil palm yield is 27.7 Mg ha^{-1}. An EC tower (22 m height)
140 is situated in the center of the site with a fetch of up to 500 m in each direction (Meijide et al., 2017) (Fig.
141 1).

142
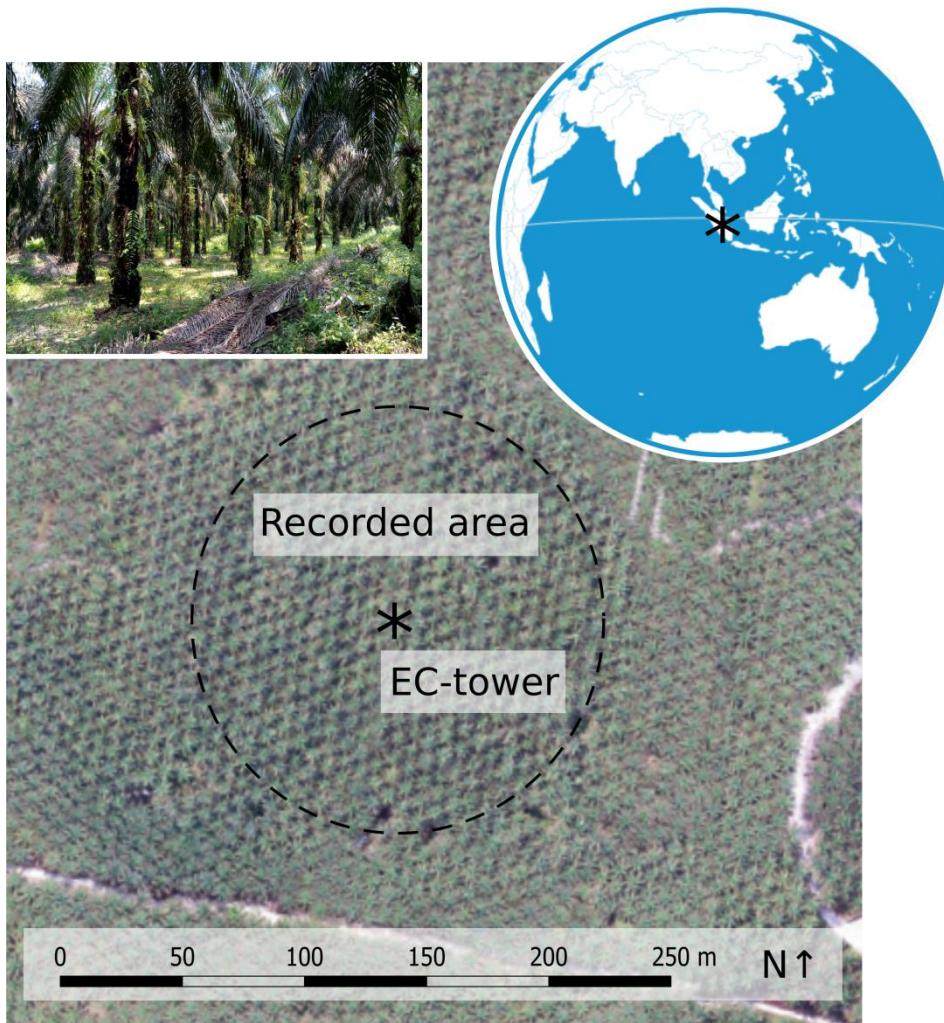
Figure 1: The study site in a mature commercial oil palm plantation in the lowlands of Jambi province, Sumatra, Indonesia.

145

2.2 Drone-based image acquisition

147

We used an octocopter drone (MK EASY Okto V3; HiSystems, Germany) equipped with a thermal and an RGB camera mounted in a stereo setup on a gimbal to ensure nadir perspective. The radiometric thermal camera was a FLIR Tau 2 640 (FLIR Systems, USA) attached to a TeAx Thermo-capture module (TeAx Technology, Germany). The sensor covers spectral bands ranging from 7.5 to 13.5 μm with a relative thermal accuracy of 0.04 K and an absolute thermal accuracy of ± 2 K (FLIRSystems, USA). The RGB camera was based on an Omnivision OV12890 CMOS-Sensor (Omnivision, USA) with a 170° FOV

fish-eye lens. Instead of the mosaicking approaches applied in most of the mentioned previous studies, we used a single image recording concept as faster image acquisition allows for a denser temporal resolution of LSTs. To capture an area of 100 m radius around the EC tower in a single shot of the thermal camera, images were taken from 260 m altitude. Image corners were removed due to vignetting effects. During a consecutive five-day flight campaign in August 2017, 61 LST data sets and matching EC measurements were recorded. Flights were conducted between 9 am and 4 pm local time, in accordance with the 30 min intervals of the EC averaging cycles, resulting in 10 to 14 flights per day. All LSTs were measured using a fixed emissivity of one as the energy balance models would introduce specific soil and vegetation emissivities in the process.

2.3 Energy balance models

LSTs are recorded as 'snapshots' representing an instantaneous state of surface temperatures. Soil-Vegetation-Atmosphere Transfer (SVAT) models use these instantaneous observations of LST to solve the energy balance equation and estimate instantaneous fluxes. In our study the one-source energy balance model DATTUTDUT (Timmermans et al., 2015) and two two-source energy balance models, TSEB-PT (Norman et al., 1995) and DTD (Norman et al., 2000), were applied. For the TSEB-PT and DTD model directional radiometric temperatures are used and no further calculation of aerodynamic temperature by using an excess resistance term is needed (Hoffmann et al., 2016). Using drones, the proximity of the thermal camera to the surface is much closer compared to other typical carriers (such as satellites or planes) and hence atmospheric effects are supposed to have only a very minor effect. To use a uniform input for all the applied models, we used directional radiometric temperature recordings from the drone as input without applying further corrections. All models in this study use instantaneous land surface temperatures (LST) to solve the energy balance equation:

$$R_n = G + H + LE \qquad \text{(eq. 1)}$$

Where R_n is the net radiation, G is the ground heat flux and the turbulent fluxes H and LE represent sensible and latent heat flux, respectively. R_n is estimated by calculating the budget of incoming ($\downarrow$) and outgoing ($\uparrow$) long- (l) and short-wave (s) radiation:

$$R_n = R_s\downarrow + R_s\uparrow + R_l\downarrow + R_l\uparrow = (1-\alpha) * R_s\downarrow + \varepsilon_{surf} * \varepsilon_{atm} * \sigma * T_{air}^4 - \varepsilon_{surf} * \sigma * T(\theta)_{surf}^4 \qquad \text{(eq. 2)}$$

Where the short-wave component is calculated by multiplying incoming short-wave radiation $R_s\downarrow$ [W m^{-2}] with its absorption ratio deducted from the combined soil and vegetation albedo α. This way, reflected outgoing short-wave radiation $R_s\uparrow$ is subtracted from the energy balance. The long-wave radiation budget is calculated from surface (soil and vegetation) emissivity ε_{surf} and atmospheric emissivity ε_{atm}, the Stefan-

Boltzmann constant σ ($5.6704*10^{-8}$ W m^{-2}*K^{-4}), air temperature T_{air} and radiometric land surface temperature $T(\theta)_{surf}$ (both in K). The incoming long-wave radiation component is added to the budget and the outgoing long-wave radiation is component subtracted.

2.3.3 DATTUTDUT

Key input for the DATTUTDUT model is a LST map from where the hottest and the 0.5% quantile of coldest pixels are extracted, assuming that hot pixels are a result of very little to no evapotranspiration and cold pixels origin in a high evapotranspiration rate (Timmermans et al., 2015). Fully modeled Rn is calculated based on down-welling short-wave radiation estimates calculated using sun-earth geometry to solve eq. 2. Surface albedo P_0 is calculated as in Timmermans et al. (2015) based on the assumption that dense vegetation appears colder than rocks or soil in the thermal imagery (Brutsaert, 1982; Garratt, 1992):

$P_0 = 0.05 + ((T_0 - T_{min}) / (T_{max} - T_{min})) * 0.2$ (eq. 3)

Down-welling shortwave radiation $R_s\downarrow$ is calculated from the dimensionless atmospheric transmissivity τ and the exo-atmospheric shortwave radiation $SW_{exo}= 1360$ W m^{-2} (Timmermans et al., 2015). Transmissivity τ is calculated as described in Burridge and Gadd, A.J. (1977) using the solar elevation angle α that was determined from the geographic position of our site and the coordinated universal time (UTC) of the measurements:

$\tau = 0.6 + 0.2 * \sin(\alpha)$ (eq.4)

$R_s\downarrow = \tau * SW_{exo}$ (eq. 5)

Timmermans et al. (2015) suggest using a constant value of 0.7 for τ and 0.8 atmospheric emissivity (ε_{atm}), but as our flight times range from 09:00 to 16:30h local time we decided to include the solar elevation angle as in eq. 4. Further, we used a constant surface emissivity (ε_{surf}) of 0.98 as recommended for vegetation dominated areas (Jones and Vaughan, 2010) and not 1.0 as simplified in the original formulation of the DATTUTDUT model. Air temperature T_{air} was calculated as the 0.5% quantile of the coldest pixels in the image.

As the original DATTUTDUT formulation doesn't account for cloud cover, eq.5 is replaced by measured short-wave irradiance as in Brenner et al. (2018) for model runs with Rn_sw. For model runs with Rn_mes eq. 2 was replaced by R_n measurements recorded at the EC-tower.

The sum of the turbulent fluxes is calculated by subtracting G from R_n. The result is fractioned into its

228   components H and LE, using the evaporative fraction (EF) (Timmermans et al., 2015):

229

230    $EF = LE / (LE+H) = LE / (R_n - G) = (T_{max} - T(\theta)_{surf}) / (T_{max} - T_{min})$ (eq. 6)

231

232   For our implementation of the DATTUTDUT model we used the QGIS3 plugin QWaterModel (Ellsäßer

233   et al., 2020) that is provided with an easy-to-use graphical user interface.

234

235   TSEB-PT

236

237   TSEB-PT calculates surface-energy budgets from the recorded LSTs splitting observations into a canopy

238   and a soil fraction (Norman et al., 1995; Song et al., 2016; Xia et al., 2016). The model consists of two

239   parts: First an initialization part where all parameters that do not depend on soil and canopy temperature

240   partition and knowledge of atmospheric stability are computed. Afterwards an iterative part where the

241   Monin-Obukhov length is stabilized and the fluxes are finally derived. To begin this process vegetation

242   cover $f_c(\theta)$ is computed as in (Campbell and Norman, 1998):

243

244    $f_c(\theta) = 1 - \exp((-0.5\Omega(\theta) * LAI) / (\cos(\theta)))$ (eq. 7)

245

246   where LAI is leaf area index, θ is the sun zenith angle and Ω is a nadir view clumping factor to represent

247   the cross-row structure in which the oil palm is planted (Kustas and Norman, 1999). Guzinski et al. (2014)

248   suggest a maximum limit of 0.95 for $f_c(\theta)$, so that a small fraction of the soil is still visible and extreme

249   magnitudes for soil temperature are avoided. Roughness parameters are calculated from vegetation height.

250   T_{air} was measured at the EC-tower, $T(\theta)_{surf}$ was recorded with the drone both similar to descriptions in

251   (Hoffmann et al., 2016). For the two-source energy balance models we used a canopy emissivity of 0.98

252   and soil emissivity of 0.95. The emissivity values are based on averages for the 8-14 μm spectrum taken

253   from Jones and Vaughan, (2010). The TSEB-PT model requires additional in situ meteorological

254   measurements of long- and short-wave radiation, wind speed, barometric pressure and relative humidity,

255   which in our case were recorded at the EC tower. Further, measured data on LAI as well as surface and

256   canopy albedo are required. The three resistances in the soil-canopy-atmosphere heat flux network, the

257   aerodynamic resistance to heat transport (RA), the resistance to heat transport from the soil surface (RS)

258   and the total boundary layer resistance of the leaf canopy (RX) are calculated as in (Norman et al., 1995,

259   2000). Net radiation and the three resistances remain constant during the model runs. After finishing the

260   computation of all constant parameters, the iterative part of the model starts assuming Monin-Obukhov

261   length tends to infinity. In the first iteration R_n is partitioned into a soil and canopy fraction by calculating

262   net radiation divergence ΔR_n (Hoffmann et al., 2016; Norman et al., 2000):

263

264    $\Delta R_n = R_n * (1 - \exp((-K*LAI*\Omega0) / \sqrt{(2\cos(\theta_s))})$ (eq. 8)

where K is an extinction coefficient that varies according to LAI (Hoffmann et al., 2016). We are aware of the fact, that the determination of K using LAI is disputed as other studies found no significant correlation of K and LAI (Zhang et al., 2014). With ΔR_n known, sensible heat flux is then estimated using the Priestley-Taylor approximation following the approach by Hoffmann et al., (2016):

$$H_c = \Delta R_n * (1-\alpha_{PT} * f_G * (D/(D+\gamma))) \qquad \text{(eq. 9)}$$

α_{PT} is the Priestley-Taylor coefficient and both γ the psychrometric constant and the slope of the saturation pressure curve D were calculated as in (Allen et al., 1998). Canopy temperature T_C was computed by summing up the results of the linear approximation in equation (A7) for $T_{C,lin}$ and ΔT_C from equation (A11) both from (Norman et al., 1995). Knowing canopy temperature T_C and the fraction of view covered by vegetation f_θ as in (Hoffmann et al., 2016), soil temperature T_S can be calculated:

$$T_s = (T(\theta)_R{}^4 - f_\theta * T_C{}^4) / (1-f_\theta)^{(1/4)} \qquad \text{(eq. 10)}$$

With soil and canopy temperatures and the resistances of the soil-canopy-atmosphere heat flux network known, fluxes can be calculated with equations (9), (10), (11) and (13) from Hoffmann et al. (2016). Total latent and sensible heat fluxes are calculated as the sums of canopy and soil fluxes. In the following iterations, a recalculation of Monin-Obukhov length takes place until a stable value is reached and the resulting fluxes are derived. For the model runs with Rn_mod and Rn_mes the model net radiation is forced accordingly.

DTD

The Dual-Temperature-Difference (DTD) model works very similar to TSEB-PT and differs mainly in the way how sensible heat flux is calculated (Hoffmann et al., 2016). In the DTD model, the absolute temperatures of land surface and air (as used in the TSEB-PT) are supplemented with a second set of early morning reference measurements of LST and air temperature, thus creating a dual-temperature difference (Norman et al., 2000). The first observation is recorded in the early morning hours and the second observation is recorded later on the same day at any given time. We used two IRTs attached to the EC tower (see EC methodology Sect. 2.4 for details and Sect. 2.7 for the limitations) for the necessary early morning reference readings of absolute temperature and used the averaged LSTs to create a uniform map as input for the DTD model (similar as e.g. in Hoffmann et al. 2016). This relates measurements at any time during the day to measurements recorded in the morning, when fluxes are assumed to be minimal, and thereby accounts for measurement biases of LST (Anderson, 1997; Hoffmann et al., 2016). H flux is then calculated using the time-differential temperature and a series resistance network as it is

recommended for densely vegetated regions to consider interaction of soil and canopy fluxes (Guzinski et al., 2014; Li et al., 2005).

The actual amount of evapotranspirated water (ET_w) in mm h^{-1}was calculated as in (Timmermans et al., 2015):

$$ET_w = ((LE*t)/1000000)/(2.501-0.002361*(T_{air}-273.15)) \qquad (eq.11)$$

Where LE is the latent heat flux in W m^{-2}, t is the respective timespan in seconds and T_{air} is the air temperature in Kelvin.

2.4 Eddy covariance measurements

The micrometeorological tower is located in the center of the study site (Fig. 1). The EC technique was used to measure LE and H fluxes from high frequency (10 Hz) measurements of above-canopy water vapor concentration, sonic temperature, and 3-D wind components. The flux system consisted of a sonic anemometer (Metek uSonic-3 Scientific, Elmshorn, Germany) and a fast response open-path CO_2/H_2O infrared gas analyzer (Li-Cor7500A, LI-COR Inc. Lincoln, USA) installed at 22 m height. Meteorological variables were measured every 10 sec, averaged to 10 min means and stored on a DL16 Pro data logger (Thies Clima, Göttingen, Germany). R_n and its components were measured with a net radiometer (CNR4, Kipp & Zonen, Delft, The Netherlands) at 22 m height. Air temperature and relative humidity were measured with thermohygrometers (type 1.1025.55.000, Thies Clima, Göttingen, Germany) at 16.3 m height. Further, a wind direction sensor (Thies Clima, Göttingen, Germany) (22 m height) and 3-cup anemometers (Thies Clima, Göttingen, Germany) (18.5, 15.4, 13, and 2.3 m height) for wind speed measurements were installed on the tower. The two IRTs used in our study (IR100 Radiometer, Campbell Scientific Inc., Logan, USA) have a field-of-view (FOV) of 8-10°. Considering the distance from their fixed location on the tower to the average height of the oil palm canopy, they cover a circular area of 2.2 m^2, over which they average the received thermal signal. The recorded canopy area comprises different functional parts of the canopy (e.g. leaflets, petioles). On average, we assumed a surface emissivity of 0.98 for the canopy area (Jones and Vaughan, 2010). We did not correct the values recorded with the IRTs for any other influences since the distance from the canopy surface to the sensors was only about 10 m. Ground heat flux was measured using heat flux plates (HFP01, Huxeflux, Delft, The Netherlands) at 10 cm depth. Additional soil moisture and temperature measurements (Trime-Pico 32, Imko, Ettlingen, Germany) above the heat flux plate at 5 cm depth were used to calculate heat flux at the soil surface. EC data recording, filtering and processing were carried out identical to the methodology described in Meijide et al. (2017) for the same study site. As the applied drone-based models all assume full energy balance closure, we used the Bowen ratio closure method (Pan et al., 2017; Twine et al., 2000) to compute full closure for the EC measurements. The Bowen ratio method was found to produce the most congruent

results in conjunction with drone-based latent heat flux estimates (Brenner et al., 2017) and was therefore applied in this study. The energy balance closure (EBC) of the reference EC measurements was 0.77 (r^2= 0.87), which is in line with EBC reported for other tall vegetation canopies (Stoy et al., 2013). Since the used energy balance models assume full EBC, we applied the so-called Bowen ratio closure method to the EC data (Pan et al., 2017). The method assumes that wind measurements miss some of the total covariance and dispersive fluxes. Therefore, underestimations of LE and H are carried over proportionally because of similarity among fluxes (Twine et al., 2000). The Bowen ratio closure method proportionally assigns the underestimated turbulent energy to LE and H fluxes to reach full EBC.

EC data processing and quality checks were performed following the methodology described in (Meijide et al., 2017). Following (Mauder and Foken, 2006), flux estimates during low turbulence and thus stable atmospheric conditions were removed from the analysis; however, low turbulence mainly occurred during night hours and was not observed during the daytime drone flights. Generally, the EC method is associated with uncertainties of 5 - 20% (Foken, 2008). Further limitations are the high costs and quite specific requirements regarding size and terrain of the study site.

2.6 Statistical analyses

Both methods, the reference EC technique and the drone-based estimates, are associated with a certain degree of uncertainty. To account for the uncertainty in both, a model II Deming regression (Deming, 1964) was applied for the analysis to consider uncertainties in both x and y variables (Cornbleet and Gochman, 1979; Glaister, 2001). We assumed that the error ratio ($\sigma\varepsilon^2/\sigma\delta^2$) of the variances ($\sigma$) of errors on y ($\varepsilon_i$) and on x ($\delta_i$) would not differ from 1 which is the standard procedure if both uncertainties are unknown (Legendre and Legendre, 2003). We used the interquartile range method with a factor k=1.5 to remove outliers from the regression. A Durbin-Watson test was applied to test for correlation in error terms. We checked for heteroscedasticity visually and using a White test. Normal distribution of error terms was tested visually plotting standardized residuals vs. theoretical quantities and performing a Shapiro-Wilk test. Standard errors and confidence intervals for slope and intercept of the Deming regression were calculated using analytical methods (parametric) and the jackknife method (Armitage et al., 2001; Linnet, 1993). As further supporting indicators of model performance, we calculated the coefficients of determination (r^2), the Mean Absolute Error (MAE), the Root Mean Square Error (RMSE) and slope and intercept from the Deming regression. Statistics such as r^2 have their limitations in method comparison since they are designed to indicate how well the resulting model of the regression describes the outcome and are not necessarily a good measure for systematic bias between methods. However, they are used as a statistic in this study since they represent an additional indicator for interpretation. Linearity was checked visually plotting residuals vs. fitted values.

All modeling procedures and parts of the statistical analyses were computed using Python version 3.7.1 (Python Software Foundation), involving the libraries NumPy 1.14.2, SciPy 1.1.0, pandas 0.23.1, scikit-

learn 0.19.1, gdal 2.3.2, Astropy 3.2.2 and tkinter 8.6. The Deming regression was computed using the MethComp and mcr v2.2.1 package (Manuilova et al., 2014) in R version 3.6.1 (R Development Core Team, 2019). Graphic representation was processed in Python using the Matplotlib 3.0.2 and Seaborn 0.9.0 libraries.

2.7 Dataset characteristics

The dataset offers a comparatively high number of replicates from 61 drone recording flights and the corresponding eddy covariance measurements enabling a method comparison which requires at least n=60 observations (Legendre and Legendre, 2003). The data was recorded in a 30 min frequency, to facilitate the analysis of daily courses of evapotranspiration behavior creating a trade-off situation of more flights per day with shorter flight times per flight. Because flight times were so short, only a smaller footprint with a radius of 100 m around the eddy covariance station was covered, while the footprint recorded with the eddy covariance system ranged up to a 500 m radius around the tower. Therefore, the reduced area of the drone recorded LST maps is often smaller than the extent of the eddy covariance footprint. We have several reasons to assume that this doesn't cause major problems for the comparison though: the study area is very homogenous with an elevation difference of 5 m in the eddy covariance footprint and the biosphere is strongly dominated by only one species (oil palm). The plantation is very well managed, so that all oil palm canopies are alive, no oil palms have died and only dry leaves are removed. A further limitation of the dataset is the lack of morning or night LST measurements that could not be recorded with the drone due to security concerns and limited access to the plantation at night. This doesn't affect the procedure of the DATTUTDUT and TSEB-PT model, but morning measurements are an important factor for the DTD model. We were able to record night and morning measurements with two stationary infrared thermometers (IRTs) that were attached to the tower. As for the DTD model, morning and later recordings should ideally be recorded with the same camera. To check whether the two IRTs measure similar temperatures compared to drone recorded LSTs, we extracted a total of 122 'IRT-footprint-sized' (i.e.~2.2 m^2) LST footprints from the drone-recorded maps. A correlation of both temperature measurements revealed a small deviation of the measured temperatures resulting in a mean absolute error (MAE) and root mean squared error (RMSE) of 1.59 and 2.15 K respectively. Since LST measurements are subject to a certain degree of uncertainty and thermal cameras usually have a measurement error of up to ±1°C (Aubrecht et al., 2016) we decided to use the morning measurements from the tower IRTs as input for the morning temperature reference. The implementation of the DTD model is therefore strictly experimental and has to be interpreted with the uncertainties of the morning measurements in mind.

410

3 Results

3.1 Meteorology

During our 61 flight missions, cloudiness was variable from clear sky to full cloud cover; short-wave irradiance ranged from 204 to 1110 W m^{-2}. The prevailing wind direction was from north-east, at an average wind speed of 1.7 m s^{-1}. Canopy air temperature ranged from 22.5 to 32.3°C and relative humidity varied between 62 and 99%. Temperature differences between measured air temperature at 16.3m (top of canopy) and mean land surface temperatures ranged from 0.005K to a single peak of 8.689K for the single flights while the daily averaged differences ranged from 1.32K to 2.13K. The energy balance closure of the reference EC measurements was 0.77 ($r^2 = 0.87$).

3.2 Drone-based modeling methods vs. eddy covariance method

At the time of the drone flights, LE from the EC method ranged between 87 and 596 W m^{-2} (mean: 337 W m^{-2}) and eddy covariance-derived evapotranspiration was on average, 0.43 ± 0.21 mm h^{-1}, with peak evapotranspiration of up to 0.87 mm h^{-1} during midday. Congruence of LE estimates with reference EC measurements differed among the three applied models and was further affected by the configuration of the R_n assessment (Fig. 2). The assumptions for Rn_mod were not always met as cloud cover was present during several flights; consequently, the corresponding net radiation estimates were too high, leading to a substantial overestimation especially of smaller latent heat fluxes. The short-wave irradiance based Rn_sw configuration resulted in R_n estimates that were by average very comparable with the measured net radiation Rn_mes but also showed a rather high variation (Fig. 2). Generally, error metrics were reduced and agreement was increased the more measurement-controlled the R_n determination process was.

438
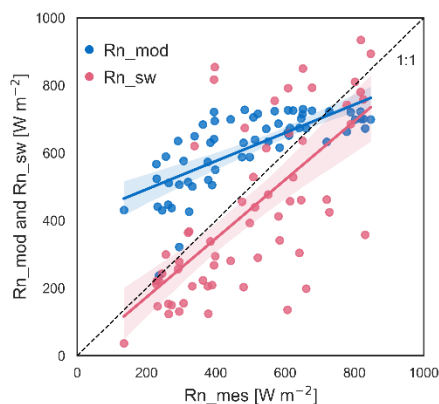
Figure 2: Measured net radiation (Rn_mes) plotted against fully modeled net radiation (Rn_mod) and net
radiation estimates based on short-short wave irradiance (Rn_sw).

DATTUTDUT LE estimates closely agreed with EC measurements around noon, but were higher in the
morning and afternoon hours, which is caused by overestimations of R_n from the Rn_mod method (Fig.
3a). LE estimates from TSEB-PT were consistently higher than EC measurements, with particularly large
divergences around noon (Fig. 3a). The LE predictions from the DTD model in Rn_mod configuration
were rather overestimated, especially around noon when compared with the EC reference measurements
(Fig. 3a). Models with Rn_sw configuration produced LE estimates that matched LE from EC more
closely (Fig. 3b). DATTUTDUT computed similar or higher estimates of LE compared to the EC
measurements during noon but mostly underestimated LE fluxes in the morning and afternoon, while
TSEB-PT produced more congruent LE estimates for the morning and afternoon hours but also
overestimated LE fluxes especially during noon (Fig. 3b). The DTD model showed a very similar pattern
with overestimations of LE fluxes around noon and more accurate estimates for morning and afternoon
hours (Fig. 3b). Both two-source energy balance models with Rn_sw configuration yielded comparably
accurate estimates during the morning and afternoon hours. With Rn_mes configuration, DATTUTDUT
computed closely matching LE estimates at all times of day across the five-day measurement period,
while TSEB-PT and DTD consistently produced much higher estimates than EC around noon but
otherwise calculating mostly accurate results (Fig. 3c).

457
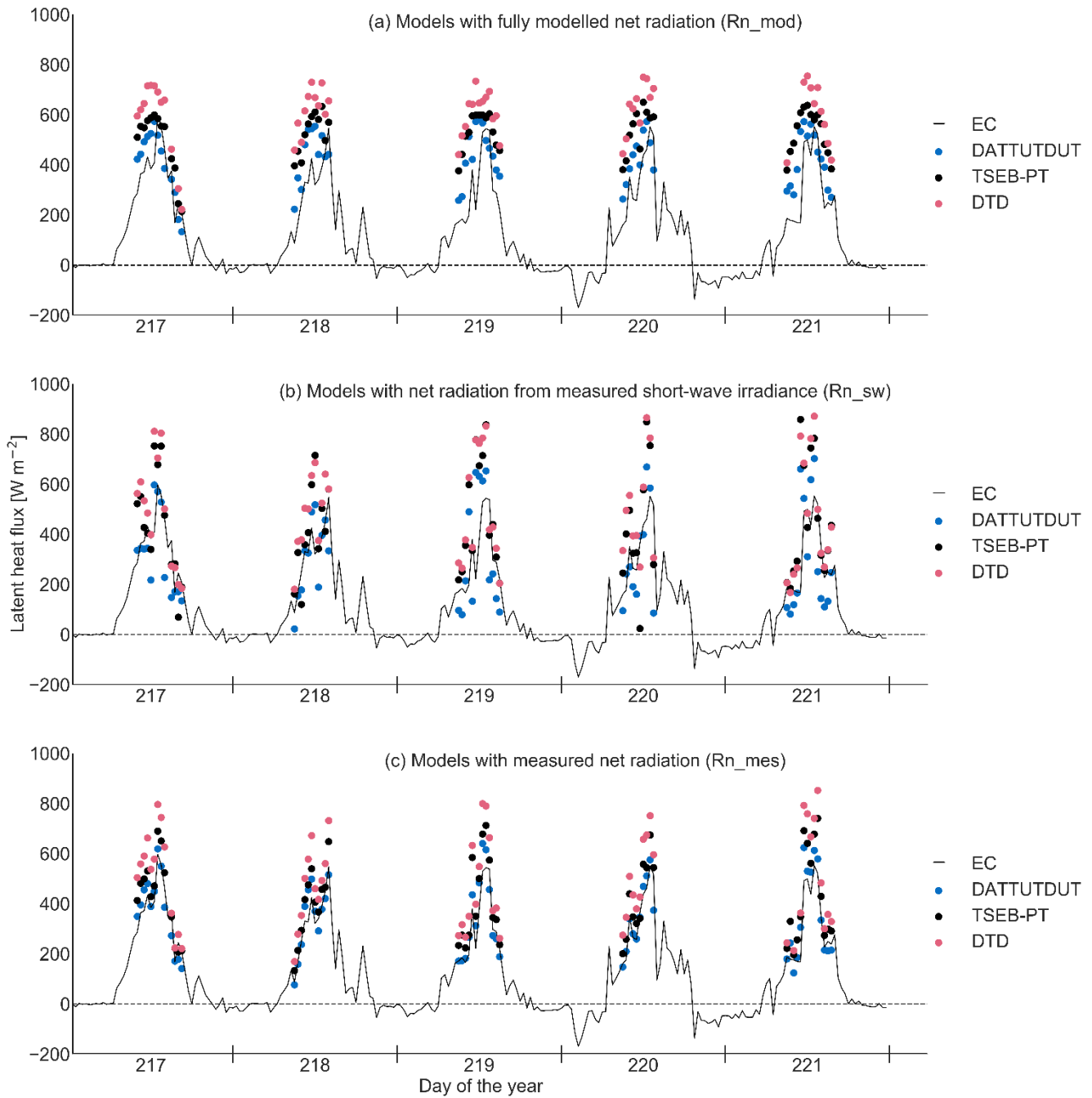
Figure 3: Latent heat flux (LE) from energy balance models (DATTUTDUT, TSEB-PT, DTD) and three different configurations of net radiation (R_n) determination (Rn_mod, Rn_sw, Rn_mod) and eddy covariance measurements (EC) over five consecutive days (n = 61 flight missions).

Across all daytimes and weather conditions (n=61 flight missions), congruence among drone-based LE estimates and reference EC measurements was highest for the DATTUTDUT model with Rn_mes configuration (r^2=0.85); MAE and RMSE were 47 and 60 W m^{-2}, respectively (Fig. 4). To compare the model predictions and the eddy covariance measurements, we computed a Deming regression between both LE predictions from the models and LE estimates by the EC method. The methods are considered to be statistically interchangeable if the confidence intervals of the slope and intercept include one and zero respectively. If the confidence intervals for the intercept of the Deming regression include zero, there is no constant or continuous error between the two methods. If the confidence intervals for the intercept do not include zero, both methods differ by a constant amount, i.e. the new method has a continuous error compared to the reference method. In contrast, the confidence intervals of the slope of the Deming regression indicate whether there is a proportional error between the methods, which increases proportionally with the magnitude of the predicted value. Deming regression of the LE estimates of the DATTUTDUT model with Rn_mes configuration showed no significant proportional or constant error compared to EC measurements as the values one and zero lay within the respective 99% confidence interval ranges of slope and intercept (Fig. 5). It is thus indicated that there is no significant difference between LE estimates from DATTUTDUT with Rn_mes configuration and the EC technique. The TSEB-PT model in Rn_mes configuration also showed no significant continuous errors but was subject to a minor proportional bias (Fig. 5c). The TSEB-PT model overestimated LE particularly around noon, when fluxes are very high (Fig. 3c and 4c). The DTD model also showed no continuous bias but indicated a proportional error in the analytical method and the Jackknife method (Fig. 5c). In the Rn_sw configuration, only the DATTUTDUT model showed no significant proportional and continuous error of LE estimates compared to EC measurements (Fig. 5b). TSEB-PT and DTD model estimates showed no significant constant deviation from the EC measurements but were subject to a proportional error (Fig. 4b and 5b). However, all confidence intervals for models with the Rn_sw configuration were rather wide indicating a large level of uncertainty. All models in the Rn_mod configuration showed significant proportional and constant errors or large biases compared to EC measurements, as well as very large confidence intervals Fig. 4a and 5a).
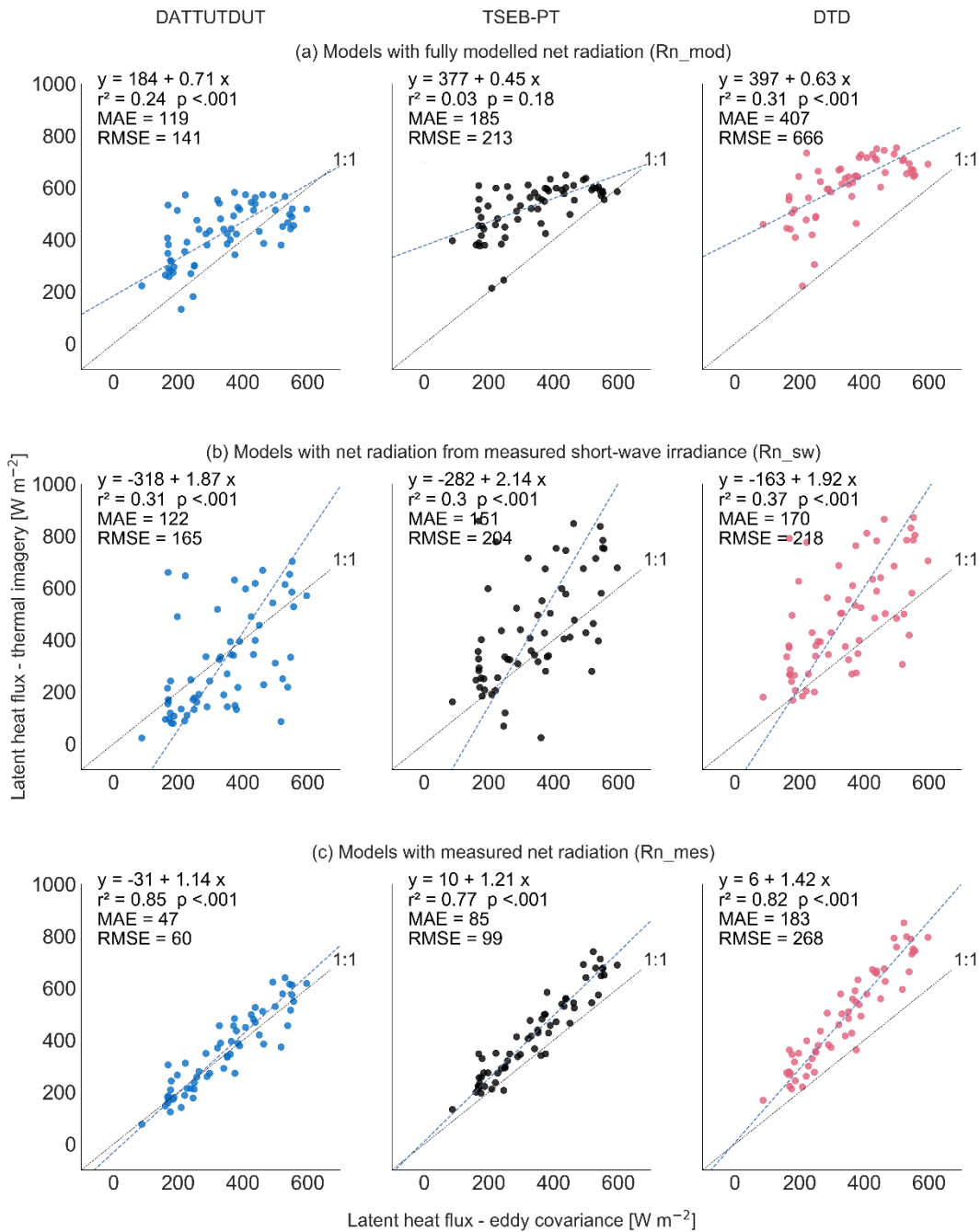
Figure 4: Model II Deming regression of latent heat flux estimates from drone-based energy balance models (DATTUTDUT, TSEB-PT, DTD) and different configurations of net radiation (Rn_mod, Rn_sw, Rn_mes) with the eddy covariance method (n = 61 flight missions).

496
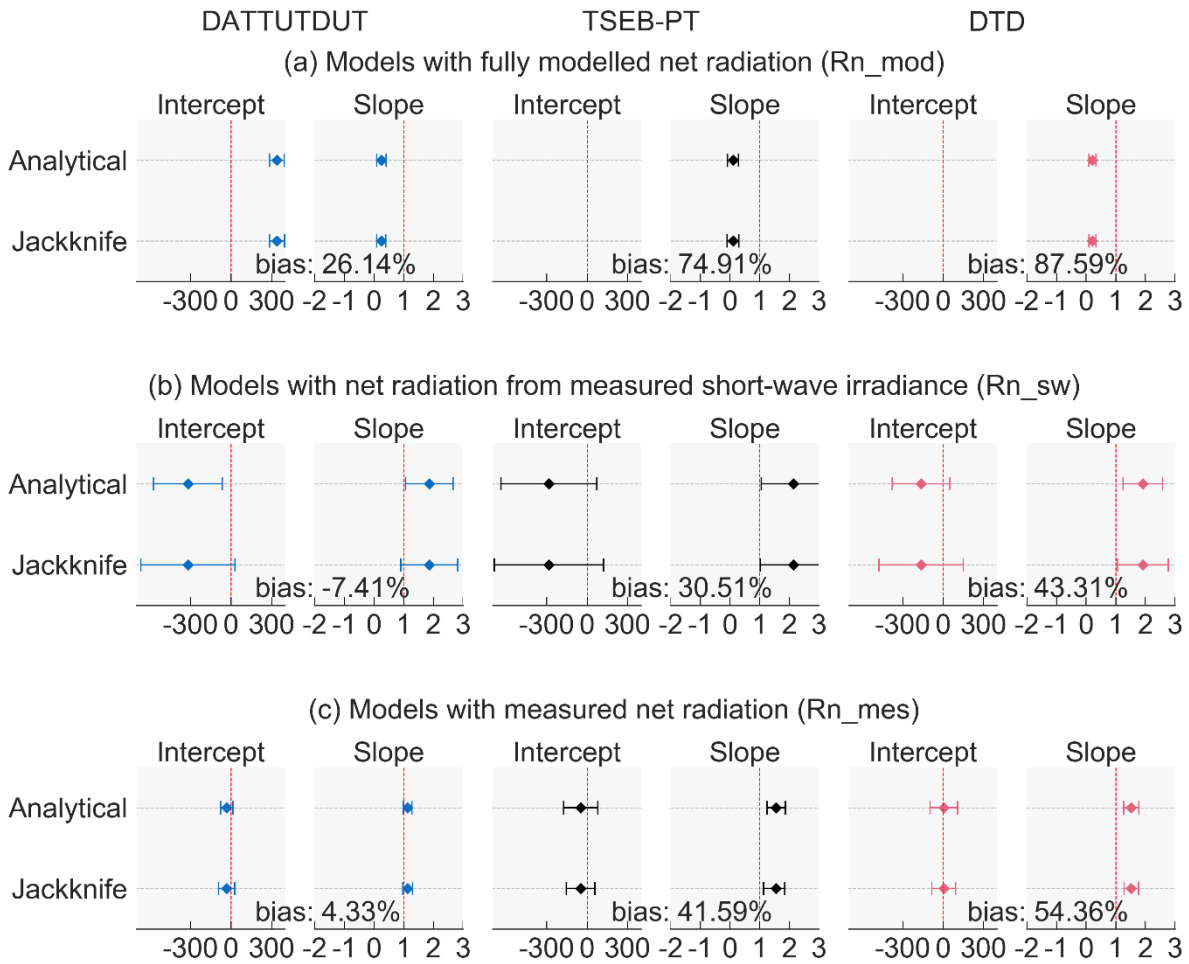
Figure 5: Confidence intervals for intercept and slope of Deming regression for the different LE
estimation approaches compared with EC measurements. X-level for the bias is the mean of the
established EC reference method. The intercept is displayed in W m^{-2}.

3.3 Spatial distribution of LE

For 9th of August 2017, 12.30 h, the DATTUDUT in Rn_mes configuration suggested a mean of 526 W
m^{-2} (minimum of 0 on the corrugated iron roof of the EC tower system, maximum of 637 W m^{-2},
coefficient of variation 7.53 %, for the analyzed 18,383 pixels) (Fig. 6), which translates to a mean ET of
0.778 mm m^{-2} h^{-1}. Locally, i.e. in the center of oil palm crowns, high LE of $>$ 400 W m^{-2} was observed,
while LE from soil and ground vegetation areas between oil palm canopies was lower. The LE fluxes of

508   all pixels were almost normally distributed for the one-source energy balance model DATTUDUT (Fig.
509   7), whereas the distribution of the two-source energy balance model TSEB-PT (for the same LST dataset)
510   was more skewed, with more LE observations at the upper end of the range. The spatial LE estimates
511   from the DTD model resulted in a similar distribution than from the TSEB-PT model (Fig. 7). Both
512   distributions of the two-source energy balance models show gaps in the histogram, while the histogram
513   of the DATTUTDUT model displays a more continuous distribution (Fig. 7)

514
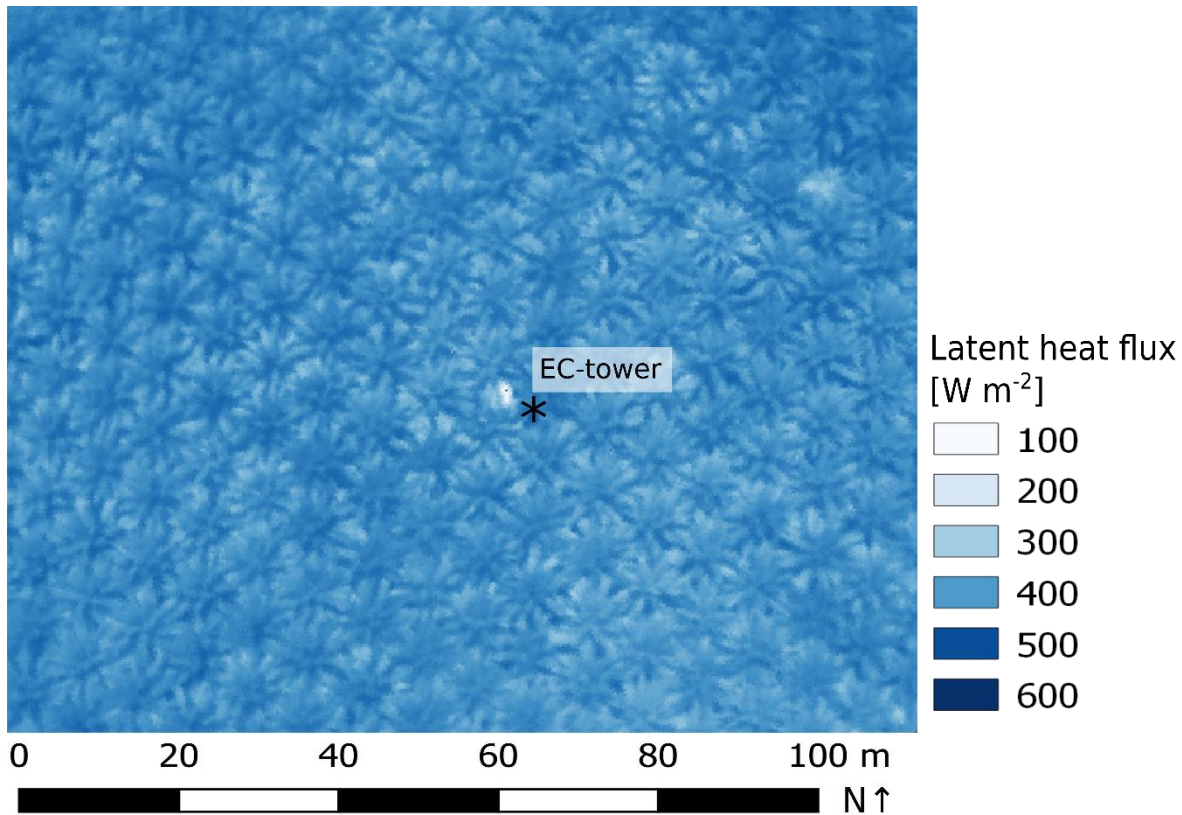
515

516   **Figure 6:** Spatial distribution of latent heat flux from drone-based thermography and subsequent energy
517   balance modeling (DATTUTDUT with Rn_mes configuration, 9 August 2017, 12.30 h).
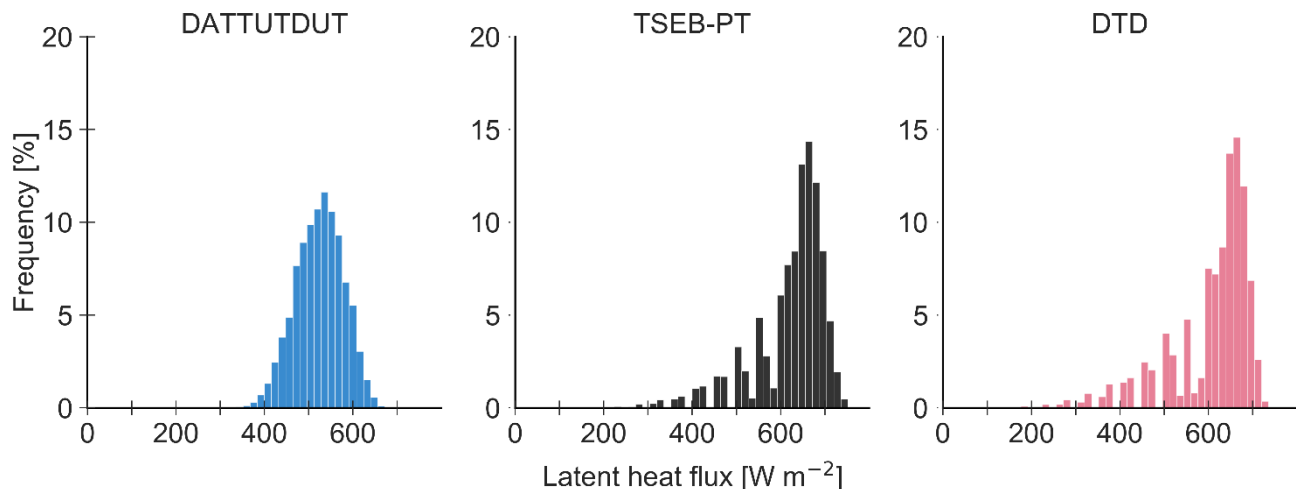
Figure 7: Frequency distribution of latent heat flux for the model output images from the same thermal image as shown in Fig. 5 (9 August 2017, 12.30 h). Absolute histogram bin size was set to 16 W m^{-2}, we used 50 bins from 0 to 800 W m^{-2}.

4 Discussion

Our study indicates a high agreement between latent heat fluxes assessed by drone-based thermography and the eddy covariance technique. However, the performance of the three applied energy balance models differed among each other and among different configurations of net radiation assessments in the models (Fig. 3 and 4). Model II Deming regression analyses and associated quality assessments suggest interchangeability between the DATTUTDUT model in Rn_mes configuration and the EC technique (Fig. 4 and 5). Applying this configuration, a fine grain spatial analysis of latent heat fluxes suggests relatively low heterogeneity of LE in the studied tropical oil palm plantation (Fig. 6).

4.1 Drone-based LE modeling vs. eddy covariance measurements

The confidence intervals of slope and intercept of the Deming regression indicate that the one-source energy balance model DATTUTDUT with Rn_mes configuration is statistically interchangeable with the established EC method for estimating LE fluxes. There are advantages and limitations to both methods. For example, the DATTUTDUT model provides insights on the spatial distribution of LE fluxes within the full extent of the available LST maps, whereas the EC technique averages the LE fluxes within its footprint to a single value. On the other hand, the DATTUTDUT model is temporally limited to the availability of LST maps, whereas the EC method can measure fluxes continuously over several years

once the equipment is in place. The DATTUTDUT model with Rn_mes configuration further requires additional measurements of short- and long-wave radiation. In our study, these measurements were taken with the EC equipment, but future stand-alone drone approaches are possible by using on-board miniaturized radiation sensors (Castro Aguilar et al., 2015; Suomalainen et al., 2018). However, the accuracy of such on-board radiation sensors should first be tested against reference methods, e.g. visually by scatter or inter-comparison plots (Castro Aguilar et al., 2015; Suomalainen et al., 2018) or with a model II regression procedure evaluating the interchangeability of methods and measurements (Passing and Bablok, 1983). The two-source energy balance models TSEB-PT and DTD in the Rn_mes configuration showed a very similar behavior. Both were found to have no continuous error when compared to the reference EC method. However, a small bias towards the overestimation of relatively high fluxes around noon was observed, which might be removed by improving the balance of e.g. vegetation parameters for oil palm.

All models with the Rn_sw configuration showed a significant proportional error compared to EC measurements, which was mainly rooted in the high variance of the Rn_sw configuration. The short-wave irradiance measurements used in this study were stored as 10 min averages that probably didn't represent the high level of irradiance variations in the tropical study area adequately. Previous studies have pointed out that R_n derivation based on short-wave irradiance measurements is challenging as long-wave radiation budgets are often completely independent from their short-wave counterparts (Hoffmann et al. 2016). Estimation errors in long-wave radiation budgets have e.g. been reported to be related to high relative air humidity, when some of the original model assumptions are no longer met (Hoffmann et al., 2016). We observed a negative correlation ($r^2 = 0.46$) between incoming long-wave irradiance and relative humidity and assume that the high relative humidity in our tropical study area may have affected the determination of R_n when using the Rn_sw configuration through inaccuracies in estimating long-wave radiation budgets, therefore causing the observed significant continuous errors. Since we recorded the data during very different daytimes and weather situations, the short-wave irradiance based approach might not be the most adequate mean of R_n derivation. However, this approach can be very useful for measurements without the presence of clouds or high levels of relative humidity. We thus also consider the Rn_sw configuration valuable for future research, particularly because measurements of incoming short-wave radiation are much easier to implement than assessing complete short- and long-wave radiation budgets as necessary for the Rn_mes configuration. The application of the Rn_sw configuration for a one-source energy balance model such as DATTUTDUT was also tested in two previous studies, with similar results to our study, i.e. a reduction of errors compared to its original formulation with fully modeled Rn_mod (Brenner et al., 2018; Xia et al., 2016).

Lastly, the model configuration Rn_mod did not produce accurate LE estimates for all three models, as many of the basic assumptions for fully modelled R_n determination are not met in tropical environments such as our equatorial study area. As such, the sky is often cloudy, while haze frequently occurs during periods without rainfall. Even if no clouds are visible, relative humidity is often high, which interferes

with the clear-sky assumptions of the Rn_mod configuration (Still et al., 2019).

Among the three models applied in our study, the relatively simple DATTUTDUT model produced the most precise LE estimates compared to eddy covariance reference measurements. Similar conclusions were reached by Brenner et al. (2018), where DATTUTDUT marginally outperformed the more complex TSEB-PT model. On the other hand, contrasting observations were made by Xia et al. (2016) in vineyards with more extreme temperature divergences between soil and vegetation, where the TSEB-PT model produced more precise estimates of LE than the DATTUTDUT model. This was explained by the better physical representation of energy and radiative exchange in the TSEB-PT model. The authors further point out that R_n determination is not the only source of error in the DATTUTDUT model (Xia et al., 2016). In our study, the TSEB-PT model slightly outperformed the more complex DTD model in the Rn_mes configuration regarding error terms. Limitations of the presented methods compared with the reference EC method however still exist. As such, the thermography-based recording process for land surface temperatures can be affected by water vapor, haze or dust, which increase atmospheric emissivity. Also, wind and turbulence cooling effects that compete with evaporative cooling are not captured in this approach.

We used the Bowen-ratio method to close the energy balance for the reference EC measurements. As reported by Xia et al. (2016), agreement between measured EC and modeled LE estimates could potentially be increased by using the residual method from Twine et al. (2000) for energy balance closure. Further potential improvements include the aerial sampling alignment with the EC measurement logging cycles. We compared snapshot measurements of LST to 30 min averages of EC measurements for the corresponding times in an environment where key variables such as solar irradiance can change very quickly. Better matching the measurement cycle duration may further improve agreement between the methods and was already suggested in a previous study (Brenner et al., 2018). Further, in our study the aerial-derived LST images represented only the center area of the (at times quite variable and large) EC footprint. Covering the whole potential area of the footprint in all directions could also increase agreement between the measurements, but would require even higher flight altitude or longer flight times to cover the whole area; both options would reduce the number of temporal replicates and increase errors from measurements and processing, but could nonetheless be viable approaches for other research questions.

Only few previous studies have demonstrated applicability and limitations of estimating LE with the three energy balance models from non-satellite data. In these studies, LSTs were e.g. recorded from drones for European grasslands and croplands (Brenner et al., 2018; Hoffmann et al., 2016) and from drones or airplanes for taller vegetation including olive orchards and vineyards (Ortega-Farías et al., 2016; Xia et al., 2016). Our study adds to this an application of these models in a tropical environment, for higher vegetation (i.e. oil palm) and across variable daytimes and weather conditions. Generally, the equatorial study site was rather challenging due to high temperatures and humidity and frequent occurrence of haze,

as well as for logistical reasons. Additionally, many previous drone-based studies were conducted on grasslands (e.g. Brenner et al. 2017, 2018) or on low-growing crops such as wheat fields (Hoffmann et al., 2016), but not on crops with a rather complex canopy structure such as oil palm. On the other hand, our study site showed large temperature differences between soil and canopy, which simplified the distinguishing of each fraction. We further analyzed for the first time whether drone-data based models and EC measurements can be used interchangeably, as our large sample size of n=61 flights allowed for a method comparison based on a model II Deming regression (Legendre and Legendre, 2003). We conclude that this is the case for some models and configurations, above all for the DATTUTDUT with Rn_mes configuration.

4.2 Spatial distribution of latent heat fluxes

A particular strength of drone-based thermal imagery is the high spatial resolution which allows for spatially explicit assessments of evapotranspiration, within and potentially also beyond the footprints of EC towers. The outlines of the single oil palm canopies are clearly visible in the LE flux map (Fig. 6), with the highest LE fluxes occurring in the center of the oil palm canopies. We assume that this spatial pattern is caused by an increased local LAI in the centers of the oil palm canopies, while leaf area density decreases towards the outer canopies. Further, the central areas of oil palm canopies are more exposed to sunlight and wind throughout most of the day, increasing their potential for (evapo)transpiration compared to canopy edges. Mixed pixel effects (among soil and canopy) likely also contribute to the observed lower LE fluxes towards the borders of oil palm canopies. Further contributing factors to higher LE fluxes in the centers of oil palm canopies could be leaf age (with younger leaves in the center) and additional ET from pockets in the axils of pruned leaves along the stem, which contain small water reservoirs and epiphytes (Meijide et al., 2017; Tarigan et al., 2018).

While the DATTUTDUT histogram shows only few pixel values of zero and most pixels closely distributed around the mean, the TSEB-PT and DTD histograms are much wider distributed and with a much more pronounced peak. For the DATTUTDUT model mean and median are very similar indicating close to zero skewness. Such a distribution tending towards unimodality is also considered typical for landscapes where ET is highly dominated by one species (Xia et al., 2016). Both, the TSEB-PT and the DTD model show a different, more skewed distribution of LE fluxes (for the same dataset of LST), with the median of the LE estimates located between the mean and the upper end of the LE flux range. We assume that this skewness is caused by the TSEB-PT and DTD models being more sensitive to dry surfaces and hence better represent the lower LE flux from dryer soil areas.

Drone-based methods have a large untapped potential for ecological applications, e.g. regarding ecohydrological optimization in land use systems and designing the climate-smart urban landscapes of

652   the future. We see great potential in the drone-based remote sensing applications presented in this study;
653   especially when recent developments in drone-environment interaction, mobile edge computing
654   (potentially on-board of the drone) and communication technologies such as LoRaWAN (Long Range
655   Wide Area Network) or 5G are combined (Becerra, 2019; Marchese et al., 2019). Autonomous acquisition
656   of LSTs over EC stations and the surrounding areas can be supplemented by on-board and ground sensors.
657   Energy-balance models can then potentially be calculated using edge computing schemes on-board the
658   drone to enable a dense temporal resolution of LST, flux and ET maps in almost real-time. This concept
659   can e.g. be used for the attribution of fluxes in mixed species plant communities, the study of edge effects
660   in landscapes, and further be adapted e.g. to detect water stress in agriculture and forests.

661

662   **5 Conclusions**

663

664   Drone-based thermography and subsequent energy balance modeling under certain configurations can be
665   considered a highly reliable method for estimating latent heat flux and evapotranspiration; for some
666   configurations statistical interchangeability is suggested with the established eddy covariance technique.
667   They thus complement the asset of available methods for evapotranspiration studies by fine grain and
668   spatially explicit assessments.

669

670

Data availability

The final data used for the statistical tests were uploaded in Göttingen Research Online Data with a doi: https://doi.org/10.25625/IOF18T

Raw thermal images, orthomosaics and terrain data, georeferenced rasters and model configurations are available upon request to the corresponding author.

Author Contribution

The study was conceptualized by DH in cooperation with H (drone measurements) and AK in cooperation with TJ (eddy covariance measurements). FE led the writing of the paper with help from AR and DH supervised the work. FE collected and processed the drone data and CS the eddy covariance data. FE conducted data processing, model application, statistical analysis and production of plots in cooperation mainly with DH and AR. FE, DH and AR created a first version of the manuscript, which was further improved in a cooperation of all authors.

Competing interests

The authors declare that they have no conflict of interest.

Acknowledgements

This study was funded by the Deutsche Forschungsgemeinschaft (DFG, German Research Foundation) – project number 192626868 – SFB 990 (subprojects A02 and A03) and the Ministry of Research, Technology and Higher Education (Ristekdikti). We thank Ristekdikti for providing the research permit for field work (No. 322/SIP/FRP/E5/Dit.KI/IX/2016, No. 329/SIP/FRP/E5/Dit.KI/IX/2016 and No. 28/EXT/SIP/FRP/E5/Dit.KI/VII/2017). We thank our field assistants Zulfi Kamal, Basri, Bayu and Darwis for great support during the field campaigns and Edgar Tunsch, Malte Puhan, Frank Tiedemann and Dietmar Fellert for their technical support. We also thank Perseroan Terbatas Perkebunan Nusantara VI, Batang Hari Unit (PTPN6) for giving us permission to conduct our research at the oil palm plantation. We thank Mr. Nieto for publishing the code for TSEB-PT and DTD (pyTSEB) on www.github.com. Thanks to all 'EFForTS' colleagues and friends in Indonesia, Germany, and around the world.

References

Allen, R. G., Pereira, L. S., Raes, D. and Smith, M.: Crop evapotranspiration - Guidelines for computing crop water requirements - FAO Irrigation and drainage paper 56, FAO, Rome. [online] Available from: http://www.fao.org/3/X0490E/X0490E00.htm, 1998.

Allen, R. G., Tasumi, M. and Trezza, R.: Satellite-Based Energy Balance for Mapping Evapotranspiration with Internalized Calibration (METRIC)—Model, J. Irrig. Drain. Eng., 133(4), 380–394, doi:10.1061/(ASCE)0733-9437(2007)133:4(380), 2007.

Anderson, M.: A Two-Source Time-Integrated Model for Estimating Surface Fluxes Using Thermal Infrared Remote Sensing, Remote Sens. Environ., 60(2), 195–216, doi:10.1016/S0034-4257(96)00215-5, 1997.

Armitage, P., Berry, G. and Matthews, J. N. S.: Statistical methods in medical research, 4th ed., Blackwell Science, Malden, MA., 2001.

Aubrecht, D. M., Helliker, B. R., Goulden, M. L., Roberts, D. A., Still, C. J. and Richardson, A. D.: Continuous, long-term, high-frequency thermal imaging of vegetation: Uncertainties and recommended best practices, Agric. For. Meteorol., 228–229, 315–326, doi:10.1016/j.agrformet.2016.07.017, 2016.

Baldocchi, D., Falge, E., Gu, L., Olson, R., Hollinger, D., Running, S., Anthoni, P., Bernhofer, C., Davis, K., Evans, R., Fuentes, J., Goldstein, A., Katul, G., Law, B., Lee, X., Malhi, Y., Meyers, T., Munger, W., Oechel, W., Paw U, K. T., Pilegaard, K., Schmid, H. P., Valentini, R., Verma, S., Vesala, T., Wilson, K. and Wofsy, S.: FLUXNET: A New Tool to Study the Temporal and Spatial Variability of Ecosystem-Scale Carbon Dioxide, Water Vapor, and Energy Flux Densities, Bull. Am. Meteorol. Soc., 82(11), 2415–2434, doi:10.1175/1520-0477(2001)082<2415:FANTTS>2.3.CO;2, 2001.

Bastiaanssen, W. G. M., Menenti, M., Feddes, R. A. and Holtslag, A. A. M.: A remote sensing surface energy balance algorithm for land (SEBAL). 1. Formulation, J. Hydrol., 212–213, 198–212, doi:10.1016/S0022-1694(98)00253-4, 1998.

Becerra, V. M.: Autonomous control of unmanned aerial vehicles, Electronics, 8(4), 452, doi:10.3390/electronics8040452, 2019.

Berni, J. A. J., Zarco-Tejada, P. J., Sepulcre-Cantó, G., Fereres, E. and Villalobos, F.: Mapping canopy conductance and CWSI in olive orchards using high resolution thermal remote sensing imagery, Remote Sens. Environ., 113(11), 2380–2388, doi:10.1016/j.rse.2009.06.018, 2009.

Brenner, C., Thiem, C. E., Wizemann, H.-D., Bernhardt, M. and Schulz, K.: Estimating spatially distributed turbulent heat fluxes from high-resolution thermal imagery acquired with a UAV system, Int. J. Remote Sens., 38(8–10), 3003–3026, doi:10.1080/01431161.2017.1280202, 2017.

Brenner, C., Zeeman, M., Bernhardt, M. and Schulz, K.: Estimation of evapotranspiration of temperate grassland based on high-resolution thermal and visible range imagery from unmanned aerial systems, Int. J. Remote Sens., 39(15–16), 5141–5174, doi:10.1080/01431161.2018.1471550, 2018.

740   Brutsaert, W.: Evaporation into the Atmosphere. Theory, History, and Applications, Reidel Publishing
741   Co., 1982.

742   Burchard-Levine, V., Nieto, H., Riaño, D., Migliavacca, M., El-Madany, T. S., Perez-Priego, O., Carrara,
743   A. and Martín, M. P.: Adapting the thermal-based two-source energy balance model toestimate energy
744   fluxes in a complex tree-grass ecosystem, Hydrol. Earth Syst. Sci. Discuss., 1–37, doi:10.5194/hess-
745   2019-354, 2019.

746   Burridge, D. M. and Gadd, A.J.: The Meteorological Office operational 10-level numerical weather
747   prediction model (December 1975), British Meteorological Office, Bracknell, England. [online]
748   Available from: https://trove.nla.gov.au/version/9853886, 1977.

749   Campbell, G. S. and Norman, J. M.: An Introduction to Environmental Biophysics, Springer, New York,
750   New York., 1998.

751   Castro Aguilar, J. L., Gentle, A. R., Smith, G. B. and Chen, D.: A method to measure total atmospheric
752   long-wave down-welling radiation using a low cost infrared thermometer tilted to the vertical, Energy,
753   81, 233–244, doi:10.1016/j.energy.2014.12.035, 2015.

754   Clough, Y., Krishna, V. V., Corre, M. D., Darras, K., Denmead, L. H., Meijide, A., Moser, S., Musshoff,
755   O., Steinebach, S., Veldkamp, E., Allen, K., Barnes, A. D., Breidenbach, N., Brose, U., Buchori, D.,
756   Daniel, R., Finkeldey, R., Harahap, I., Hertel, D., Holtkamp, A. M., Hörandl, E., Irawan, B., Jaya, I. N.
757   S., Jochum, M., Klarner, B., Knohl, A., Kotowska, M. M., Krashevska, V., Kreft, H., Kurniawan, S.,
758   Leuschner, C., Maraun, M., Melati, D. N., Opfermann, N., Pérez-Cruzado, C., Prabowo, W. E.,
759   Rembold, K., Rizali, A., Rubiana, R., Schneider, D., Tjitrosoedirdjo, S. S., Tjoa, A., Tscharntke, T. and
760   Scheu, S.: Land-use choices follow profitability at the expense of ecological functions in Indonesian
761   smallholder landscapes, Nat. Commun., 7(1), 1–12, doi:10.1038/ncomms13137, 2016.

762   Cornbleet, P. J. and Gochman, N.: Incorrect Least-Squares Regression Coefficients in Method-
763   Comparison Analysis, Clin. Chem., (25/3), 432–438, 1979.

764   Deming, W. E.: Statistical adjustment of data, Dover Books Math. Ser., Dover Publications, 1964.

765   Drescher, J., Rembold, K., Allen, K., Beckschäfer, P., Buchori, D., Clough, Y., Faust, H., Fauzi, A. M.,
766   Gunawan, D., Hertel, D., Irawan, B., Jaya, I. N. S., Klarner, B., Kleinn, C., Knohl, A., Kotowska, M. M.,
767   Krashevska, V., Krishna, V., Leuschner, C., Lorenz, W., Meijide, A., Melati, D., Nomura, M., Pérez-
768   Cruzado, C., Qaim, M., Siregar, I. Z., Steinebach, S., Tjoa, A., Tscharntke, T., Wick, B., Wiegand, K.,
769   Kreft, H. and Scheu, S.: Ecological and socio-economic functions across tropical land use systems after
770   rainforest conversion, Philos. Trans. R. Soc. B Biol. Sci., 371(1694), 20150275,
771   doi:10.1098/rstb.2015.0275, 2016.

772   Ellsäßer, F., Röll, A., Stiegler, C., Hendrayanto and Hölscher, D.: Introducing QWaterModel, a QGIS
773   plugin for predicting evapotranspiration from land surface temperatures, Environ. Model. Softw., 130,
774   6, doi:https://doi.org/10.1016/j.envsoft.2020.104739, 2020.

775

776 Ershadi, A., McCabe, M. F., Evans, J. P. and Walker, J. P.: Effects of spatial aggregation on the multi-
777 scale estimation of evapotranspiration, Remote Sens. Environ., 131, 51–62,
778 doi:10.1016/j.rse.2012.12.007, 2013.

779 Fan, Y., Roupsard, O., Bernoux, M., Le Maire, G., Panferov, O., Kotowska, M. M. and Knohl, A.: A sub-
780 canopy structure for simulating oil palm in the Community Land Model (CLM-Palm): phenology,
781 allocation and yield, Geosci. Model Dev., 8(11), 3785–3800, doi:10.5194/gmd-8-3785-2015, 2015.

782 Fisher, J. B., Melton, F., Middleton, E., Hain, C., Anderson, M., Allen, R., McCabe, M. F., Hook, S.,
783 Baldocchi, D., Townsend, P. A., Kilic, A., Tu, K., Miralles, D. D., Perret, J., Lagouarde, J.-P., Waliser, D.,
784 Purdy, A. J., French, A., Schimel, D., Famiglietti, J. S., Stephens, G. and Wood, E. F.: The future of
785 evapotranspiration: Global requirements for ecosystem functioning, carbon and climate feedbacks,
786 agricultural management, and water resources: The future of evapotranspiration, Water Resour. Res.,
787 53(4), 2618–2626, doi:10.1002/2016WR020175, 2017.

788 Foken, T.: THE ENERGY BALANCE CLOSURE PROBLEM: AN OVERVIEW, Ecol. Appl., 18(6), 1351–
789 1367, doi:10.1890/06-0922.1, 2008.

790 Garratt, J. R.: The Atmospheric Boundary Layer, Cambridge University Press, Cambridge., 1992.

791 Glaister, P.: Least Sq. Revisit. Math. Gaz., 85, doi:https://doi.org/10.2307/3620485, 2001.

792 Göckede, M., Foken, T., Aubinet, M., Aurela, M., Banza, J., Bernhofer, C., Bonnefond, J. M., Brunet, Y.,
793 Carrara, A., Clement, R., Dellwik, E., Elbers, J., Eugster, W., Fuhrer, J., Granier, A., Grünwald, T.,
794 Heinesch, B., Janssens, I. A., Knohl, A., Koeble, R., Laurila, T., Longdoz, B., Manca, G., Marek, M.,
795 Markkanen, T., Mateus, J., Matteucci, G., Mauder, M., Migliavacca, M., Minerbi, S., Moncrieff, J.,
796 Montagnani, L., Moors, E., Ourcival, J.-M., Papale, D., Pereira, J., Pilegaard, K., Pita, G., Rambal, S.,
797 Rebmann, C., Rodrigues, A., Rotenberg, E., Sanz, M. J., Sedlak, P., Seufert, G., Siebicke, L., Soussana,
798 J. F., Valentini, R., Vesala, T., Verbeeck, H. and Yakir, D.: Quality control of CarboEurope flux data -
799 Part 1: Coupling footprint analyses with flux data quality assessment to evaluate sites in forest
800 ecosystems, Biogeosciences, 5(2), 433–450, doi:10.5194/bg-5-433-2008, 2008.

801 Guzinski, R., Anderson, M. C., Kustas, W. P., Nieto, H. and Sandholt, I.: Using a thermal-based two
802 source energy balance model with time-differencing to estimate surface energy fluxes with day–night
803 MODIS observations, Hydrol. Earth Syst. Sci., 17(7), 2809–2825, doi:10.5194/hess-17-2809-2013,
804 2013.

805 Guzinski, R., Nieto, H., Jensen, R. and Mendiguren, G.: Remotely sensed land-surface energy fluxes at
806 sub-field scale in heterogeneous agricultural landscape and coniferous plantation, Biogeosciences,
807 11(18), 5021–5046, doi:10.5194/bg-11-5021-2014, 2014.

808 Hansen, M. C., Potapov, P. V., Moore, R., Hancher, M., Turubanova, S. A., Tyukavina, A., Thau, D.,
809 Stehman, S. V., Goetz, S. J., Loveland, T. R., Kommareddy, A., Egorov, A., Chini, L., Justice, C. O. and
810 Townshend, J. R. G.: High-Resolution Global Maps of 21st-Century Forest Cover Change, Science,
811 342(6160), 850–853, doi:10.1126/science.1244693, 2013.

812

813 Hoffmann, H., Nieto, H., Jensen, R., Guzinski, R., Zarco-Tejada, P. and Friborg, T.: Estimating
814 evaporation with thermal UAV data and two-source energy balance models, Hydrol. Earth Syst. Sci.,
815 20(2), 697–713, doi:10.5194/hess-20-697-2016, 2016.

816 Jones, H. G. and Vaughan, R. A.: Remote sensing of vegetation: principles, techniques, and
817 applications, Oxford University Press, Oxford ; New York., 2010.

818 Kustas, W. P. and Norman, J. M.: Evaluation of soil and vegetation heat flux predictions using a simple
819 two-source model with radiometric temperatures for partial canopy cover, Agric. For. Meteorol., 17,
820 1999.

821 Lapidot, O., Ignat, T., Rud, R., Rog, I., Alchanatis, V. and Klein, T.: Use of thermal imaging to detect
822 evaporative cooling in coniferous and broadleaved tree species of the Mediterranean maquis, Agric.
823 For. Meteorol., 271, 285–294, doi:10.1016/j.agrformet.2019.02.014, 2019.

824 Legendre, P. and Legendre, L.: Numerical Ecology, 2/20 ed., Elsevier., 2003.

825 Li, F., Kustas, W. P., Prueger, J. H., Neale, C. M. U. and Jackson, T. J.: Utility of Remote Sensing–
826 Based Two-Source Energy Balance Model under Low- and High-Vegetation Cover Conditions, J.
827 Hydrometeorol., 6(6), 878–891, doi:10.1175/JHM464.1, 2005.

828 Linnet, K.: Evaluation of Regression Procedures for Method Comparison Studies, Clin Chem, (39/3),
829 424–432, 1993.

830 Manuilova, E., Schuetzenmeister, A. and Model, F.: mcr: Method Comparison Regression. [online]
831 Available from: https://cran.r-project.org/web/packages/mcr/index.html, n.d.

832 Marchese, M., Moheddine, A. and Patrone, F.: IoT and UAV Integration in 5G Hybrid Terrestrial-
833 Satellite Networks, Sensors, 19(17), 3704, doi:10.3390/s19173704, 2019.

834 Margono, B. A., Turubanova, S., Zhuravleva, I., Potapov, P., Tyukavina, A., Baccini, A., Goetz, S. and
835 Hansen, M. C.: Mapping and monitoring deforestation and forest degradation in Sumatra (Indonesia)
836 using Landsat time series data sets from 1990 to 2010, Environ. Res. Lett., 7(3), 034010,
837 doi:10.1088/1748-9326/7/3/034010, 2012.

838 Mauder, M. and Foken, T.: Impact of post-field data processing on eddy covariance flux estimates and
839 energy balance closure, Meteorol. Z., 15(6), 597–609, doi:10.1127/0941-2948/2006/0167, 2006.

840 Meijide, A., Röll, A., Fan, Y., Herbst, M., Niu, F., Tiedemann, F., June, T., Rauf, A., Hölscher, D. and
841 Knohl, A.: Controls of water and energy fluxes in oil palm plantations: Environmental variables and oil
842 palm age, Agric. For. Meteorol., 239, 71–85, doi:10.1016/j.agrformet.2017.02.034, 2017.

843 Norman, J. M., Kustas, W. P. and Humes, K. S.: Source approach for estimating soil and vegetation
844 energy fluxes in observations of directional radiometric surface temperature, Agric. For. Meteorol.,
845 77(3–4), 263–293, doi:10.1016/0168-1923(95)02265-Y, 1995.

846

Norman, J. M., Kustas, W. P., Prueger, J. H. and Diak, G. R.: Surface flux estimation using radiometric temperature: A dual-temperature-difference method to minimize measurement errors, Water Resour. Res., 36(8), 2263–2274, doi:10.1029/2000WR900033, 2000.

Oki, T. and Kanae, S.: Global Hydrological Cycles and World Water Resources, Am. Assoc. Adv. Sci., 313(5790), 1068–1072, doi:10.1126/science.1128845, 2006.

Ortega-Farías, S., Ortega-Salazar, S., Poblete, T., Kilic, A., Allen, R., Poblete-Echeverría, C., Ahumada-Orellana, L., Zuñiga, M. and Sepúlveda, D.: Estimation of Energy Balance Components over a Drip-Irrigated Olive Orchard Using Thermal and Multispectral Cameras Placed on a Helicopter-Based Unmanned Aerial Vehicle (UAV), Remote Sens., 8(8), 638, doi:10.3390/rs8080638, 2016.

Pan, X., Liu, Y., Fan, X. and Gan, G.: Two energy balance closure approaches: applications and comparisons over an oasis-desert ecotone, J. Arid Land, 9(1), 51–64, doi:10.1007/s40333-016-0063-2, 2017.

Passing, H. and Bablok, W.: A New Biometrical Procedure for Testing the Equality of Measurements from Two Different Analytical Methods. Application of linear regression procedures for method comparison studies in Clinical Chemistry, Part I, Clin. Chem. Lab. Med., 21(11), doi:10.1515/cclm.1983.21.11.709, 1983.

Prudhomme, C., Giuntoli, I., Robinson, E. L., Clark, D. B., Arnell, N. W., Dankers, R., Fekete, B. M., Franssen, W., Gerten, D., Gosling, S. N., Hagemann, S., Hannah, D. M., Kim, H., Masaki, Y., Satoh, Y., Stacke, T., Wada, Y. and Wisser, D.: Hydrological droughts in the 21st century, hotspots and uncertainties from a global multimodel ensemble experiment, Proc. Natl. Acad. Sci., 111(9), 3262–3267, doi:10.1073/pnas.1222473110, 2014.

Röll, A., Niu, F., Meijide, A., Ahongshangbam, J., Ehbrecht, M., Guillaume, T., Gunawan, D., Hardanto, A., Hendrayanto, Hertel, D., Kotowska, M. M., Kreft, H., Kuzyakov, Y., Leuschner, C., Nomura, M., Polle, A., Rembold, K., Sahner, J., Seidel, D., Zemp, D. C., Knohl, A. and Hölscher, D.: Transpiration on the rebound in lowland Sumatra, Agric. For. Meteorol., 274, 160–171, doi:10.1016/j.agrformet.2019.04.017, 2019.

Sabajo, C. R., le Maire, G., June, T., Meijide, A., Roupsard, O. and Knohl, A.: Expansion of oil palm and other cash crops causes an increase of the land surface temperature in the Jambi province in Indonesia, Biogeosciences, 14(20), 4619–4635, doi:10.5194/bg-14-4619-2017, 2017.

Song, L., Liu, S., Kustas, W. P., Zhou, J., Xu, Z., Xia, T. and Li, M.: Application of remote sensing-based two-source energy balance model for mapping field surface fluxes with composite and component surface temperatures, Agric. For. Meteorol., 230–231, 8–19, doi:10.1016/j.agrformet.2016.01.005, 2016.

Still, C., Powell, R., Aubrecht, D., Kim, Y., Helliker, B., Roberts, D., Richardson, A. D. and Goulden, M.: Thermal imaging in plant and ecosystem ecology: applications and challenges, Ecosphere, 10(6), e02768, doi:10.1002/ecs2.2768, 2019.

884 Stoy, P. C., Mauder, M., Foken, T., Marcolla, B., Boegh, E., Ibrom, A., Arain, M. A., Arneth, A., Aurela,
885 M., Bernhofer, C., Cescatti, A., Dellwik, E., Duce, P., Gianelle, D., van Gorsel, E., Kiely, G., Knohl, A.,
886 Margolis, H., McCaughey, H., Merbold, L., Montagnani, L., Papale, D., Reichstein, M., Saunders, M.,
887 Serrano-Ortiz, P., Sottocornola, M., Spano, D., Vaccari, F. and Varlagin, A.: A data-driven analysis of
888 energy balance closure across FLUXNET research sites: The role of landscape scale heterogeneity,
889 Agric. For. Meteorol., 171–172, 137–152, doi:10.1016/j.agrformet.2012.11.004, 2013.

890 Suomalainen, J., Hakala, T., Alves de Oliveira, R., Markelin, L., Viljanen, N., Näsi, R. and Honkavaara,
891 E.: A Novel Tilt Correction Technique for Irradiance Sensors and Spectrometers On-Board Unmanned
892 Aerial Vehicles, Remote Sens., 10(12), 2068, doi:10.3390/rs10122068, 2018.

893 Tarigan, S., Wiegand, K., Sunarti and Slamet, B.: Minimum forest cover required for sustainable water
894 flow regulation of a watershed: a case study in Jambi Province, Indonesia, Hydrol. Earth Syst. Sci.,
895 22(1), 581–594, doi:10.5194/hess-22-581-2018, 2018.

896 Timmermans, W. J., Kustas, W. P. and Andreu, A.: Utility of an Automated Thermal-Based Approach
897 for Monitoring Evapotranspiration, Acta Geophys., 63(6), 1571–1608, doi:10.1515/acgeo-2015-0016,
898 2015.

899 Twine, T. E., Kustas, W. P., Norman, J. M., Cook, D. R., Houser, P. R., Meyers, T. P., Prueger, J. H.,
900 Starks, P. J. and Wesely, M. L.: Correcting eddy-covariance flux underestimates over a grassland, Agric.
901 For. Meteorol., 103(3), 279–300, doi:10.1016/S0168-1923(00)00123-4, 2000.

902 Xia, T., Kustas, W. P., Anderson, M. C., Alfieri, J. G., Gao, F., McKee, L., Prueger, J. H., Geli, H. M. E.,
903 Neale, C. M. U., Sanchez, L., Alsina, M. M. and Wang, Z.: Mapping evapotranspiration with high-
904 resolution aircraft imagery over vineyards using one- and two-source modeling schemes, Hydrol. Earth
905 Syst. Sci., 20(4), 1523–1545, doi:10.5194/hess-20-1523-2016, 2016.

906 Zhang, L., Hu, Z., Fan, J., Zhou, D. and Tang, F.: A meta-analysis of the canopy light extinction
907 coefficient in terrestrial ecosystems, Front. Earth Sci., 8(4), 599–609, doi:10.1007/s11707-014-0446-7,
908 2014.

909